Particle Production in Reflection and Transmission Mode Laser Ablation: Implications for Laserspray Ionization

ARTICLE *in* JOURNAL OF THE AMERICAN SOCIETY FOR MASS SPECTROMETRY · APRIL 2013

Impact Factor: 2.95 · DOI: 10.1007/s13361-013-0631-z · Source: PubMed

J. Am. Soc. Mass Spectrom. (2013) 24:1108–1115
DOI: 10.1007/s13361-013-0631-z

RESEARCH ARTICLE

Particle Production in Reflection and Transmission Mode Laser Ablation: Implications for Laserspray Ionization

Thabiso Musapelo, Kermit K. Murray

Department of Chemistry, Louisiana State University, Baton Rouge, LA, USA

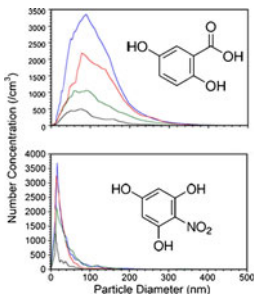

Abstract. Particles were ablated from laser desorption and inlet ionization matrix thin films with a UV laser in reflection and transmission geometries. Particle size distributions were measured with a combined scanning mobility particle sizer (SMPS) and aerodynamic particle sizer (APS) system that measured particles in the size range from 10 nm to 20 μm. The matrixes investigated were 2,5-dihydroxybenzoic acid (DHB), α-cyano-4-hydroxycinnamic acid (CHCA), sinapic acid (SA), 2,5-dihydroxy-acetophenone (DHAP), and 2-nitrophloroglucinol (NPG). Nanoparticles with average diameters between 20 and 120 nm were observed in both transmission and reflection geometry. The particle mass distribution was significantly different in reflection and transmission geometry. In reflection geometry, approximately equal mass was distributed between particles in the 20 to 450 nm range of diameters and particles in the 450 nm to 1.5 μm diameter range. In transmission mode, the particle mass distribution was dominated by large particles in the 2 to 20 μm diameter range. Ablation of inlet ionization matrices DHAP and NPG produced particles that were 3 to 4 times smaller compared with the other matrices. The results are consistent with ion formation by nanoparticle melting and breakup or melting and breakup of the large particles through contact with heated inlet surfaces.

Key words: Laser, Ablation, Ambient ionization, Ionization mechanism

Received: 20 December 2012/Revised: 23 March 2013/Accepted: 26 March 2013/Published online: 30 April 2013

Introduction

The term laserspray has been used to describe the process in which laser desorption or ablation produces highly charged macromolecular ions similar to those observed in electrospray ionization [1, 2]. Although the defining feature of laserspray is the appearance of highly charged ions, multiple charging can be achieved in a number of ways. What is now called laserspray initially used a configuration similar to atmospheric pressure matrix assisted laser desorption ionization (MALDI), and was reported as transmission mode MALDI [2]. This initial configuration used a transmission mode configuration in which the laser at high pulse energy irradiated the sample from the back side rather than the more conventional reflection mode (front-side) irradiation. Also notable is the lack of an electrical potential on the target. The temperature of the ion transfer tube is also important and temperatures above 300 °C are optimum for multiply charged ion production [1]. In subsequent studies, it was found that high pulse energy transmission mode irradiation is not a requirement for multiple charging [2]. Irradiation at atmospheric pressure is also not a requirement and multiple charging has been demonstrated with intermediate pressure (0.2 Torr) sources [3]. High vacuum ionization with multiply charged ions has been demonstrated with the matrix 2-nitrophloroglucinol (NPG) [4]. Most interestingly, the laser itself is not required and particles produced simply by forcefully striking the sample target also form highly charged ions in the mass spectrometer inlet [1].

Although rarely observed in MALDI with UV lasers, multiple charging is often seen with infrared MALDI. With a 2.94 μm Er:YAG laser, up to 13 charges were observed with caffeic acid and mouse IgG protein (ca. 150,000 Da) [5]. The propensity for multiple charging was found to be higher for proteins greater than 30 kDa in mass. Other cinnamic acid derivative matrix compounds, ferulic and sinapinic acid, were not found to produce multiple charging. Using a CO_2 laser at 10.6 μm, up to eight charges were observed with caffeic acid and mouse IgG protein [6]. With matrixes other than caffeic acid, three to four charges were observed. Multiple charging with up to six charges in positive ion mode for the protein BSA was found with a 6 ns pulse width IR OPO and a glycerol matrix but not with an Er:YAG laser at 100 ns or 185 ns pulse width [7]. In atmospheric pressure

Correspondence to: Kermit K. Murray; *e-mail:* kkmurray@lsu.edu

IR MALDI, up to 10 charges were observed for cytochrome *c* protein and up to 13 charges on myoglobin using a 2.94 μm laser and glycerol matrix. All of the IR MALDI studies were performed in reflection mode.

The mechanism proposed for ion formation in laserspray involves the production of highly charged particles that are desolvated in the heated transfer tube of the mass spectrometer [8]. In this model, the laser melts and ablates the matrix and produces liquid droplets that contain matrix and analyte. The mechanism for multiple charging is not clear, but may be non-statistical charging that has been observed for sprayed droplets [9]. The highly charged droplets are further heated in the ion transfer tube to evaporate the matrix "solvent" and multiply charged analyte ions are liberated from the particles as in the final stages of electrospray ion formation. Regardless of the specific details of the ionization mechanism, it appears that the formation of particles by laser ablation is an important component of the laserspray ionization process.

We have recently developed a method for detection and enumeration of particles formed by laser ablation that uses a combination of light scattering aerodynamic particle sizer (APS) and scanning mobility particle sizer (SMPS) that can measure particles in the size range between 10 nm and 20 μm [10]. Earlier studies with a SMPS [11] or APS [12] alone demonstrated that a large fraction of the material removed under MALDI conditions is in the form of particulate. Mid-infrared wavelengths were found to be particularly useful for particle production [13, 14]. When the SMPS and APS are used together, measurement of the full range of particle sizes reveals two major components of particle production. The smaller size component has particle diameters around 100 nm and was attributed to cluster agglomeration and hydrodynamic sputtering of the melted matrix. The larger particles have diameters around 1 μm and were attributed to melting and spallation of large chunks of the matrix.

In this work, we applied the SMPS/APS particle measurement approach to laser ablation under conditions comparable to laserspray ionization. Thin films of common crystalline MALDI and inlet ionization matrix materials were irradiated at atmospheric pressure with a pulsed 337 nm nitrogen laser in transmission and reflection mode. The particles were counted and sized using a SMPS sizing instrument in tandem with an APS instrument. Particle size and concentration in the range between 10 nm and 20 μm were measured.

Experimental

The particle ablation and sizing system used in this work has been described in detail previously [10, 12]. Two commercial particle-sizing instruments are used in tandem: an aerodynamic particle sizer (APS, model 3321; TSI, Shoreview, MN, USA) for large particles and a scanning mobility particle sizer (SMPS; model 3034; TSI) for small particles. The APS measures particles in the range of 500 nm to 20 μm and the SMPS in the 10 to 500 nm range. These instruments are used with a 240 cm^3 volume ablation chamber that is placed over the inlet of the APS and connected to the SMPS by 20 mm of 5 mm i.d. conductive plastic tubing. The chamber is at atmospheric pressure and each instrument draws in 5 L/min for a combined draw of 10 L/min that enters the chamber through a HEPA filter.

Particles were produced by irradiating samples with a 337 nm pulsed nitrogen laser (VSL-337NDS; LSI, Franklin, MA, USA) that enters the ablation chamber through a sapphire window. The sample target was a borosilicate glass microscope slide that was mounted at the center of the chamber so that the sample could be irradiated at normal incidence from the front (reflection mode) or from the back (transmission mode). A 150 mm focal length CaF_2 lens was used to focus the laser to a spot size of 300×250 μm^2. The laser pulse energy varied between 100 and 160 μJ and the laser fluence was between 1400 and 2300 J/m^2 at a repetition rate of 2 Hz.

Samples consisted of a thin film of the matrix on the microscope slide. Thin films of matrixes were prepared by depositing a 50 μL volume on the sample target and allowing it to air dry. The resulting spots were estimated to be 10 μm based on the solution concentration and spot diameter. Particle size measurements were initiated after 10 s of irradiation, to assure that a steady state of particle production and data acquired for 180 s (360 laser shots) for both reflection and transmission mode irradiation.

The matrix compounds studied were 2,5-dihydroxybenzoic acid (DHB; Sigma-Aldrich, St. Louis, MO, USA), sinapic acid (SA; Fluka, Ronkokoma, NY, USA), α-cyano-hydroxycinnamic acid (CHCA; Sigma-Aldrich), 2,5-dihydroxyacetophenone (DHAP, Sigma-Aldrich), and 2-nitrophloroglucinol (NPG; Sigma-Aldrich. The matrix solution concentrations were 40 mg/mL. The DHB and SA matrixes were dissolved in methanol (Fisher, Fair Lawn, NJ, USA); CHCA was dissolved in a 7:3 (vol/vol) mixture of acetonitrile (Fisher) and 0.1 % aqueous trifluoroacetic acid (TFA; Fisher), and the DHAP and NPG solutions were dissolved in 1:1 (vol/vol) and 0.1 % acetonitrile aqueous TFA.

Results and Discussion

Particle size measurements have been performed previously under UV MALDI conditions in reflection mode using a metal target with DHB, CHCA, and SA, but not with LSI matrices DHAP or NPG [10]. The DHAP and NPG matrices were added because they have been found to be exceptionally good for inlet ionization [15]. Of the other matrices, DHB has good performance for inlet ionization and the matrices CHCA and SA perform less efficiently.

Particle number concentration plots for the matrixes, DHB, CHCA, SA, DHAP, and NPG ablated in reflection mode are shown in Figure 1. The laser fluence was 1400,

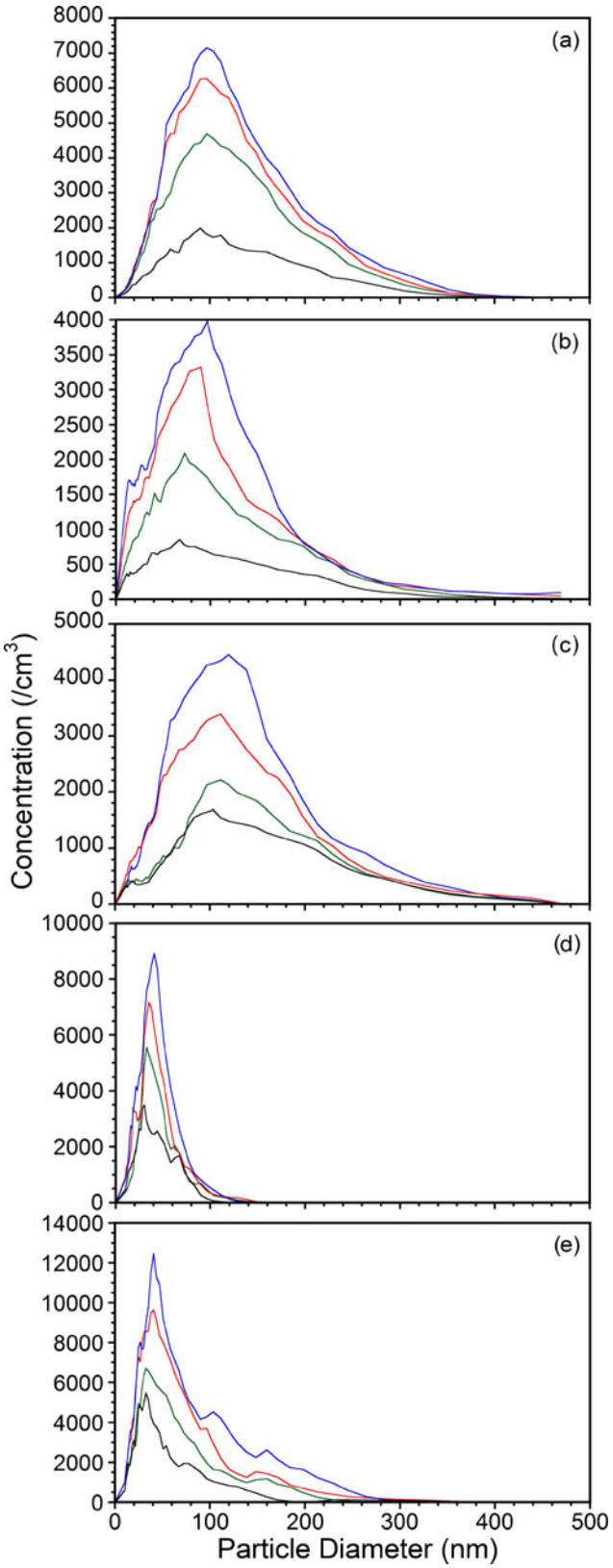

Figure 1. Reflection mode particle size distribution measured in particle count at different laser fluencies increasing from 1400 (black), 1700 (green), 2000 (red), and 2300 J/m^2 (blue) for matrices: (**a**) DHB, (**b**) CHCA, (**c**) SA, (**d**) DHAP, and (**e**) NPG

1700, 2000, and 2300 J/m^2. As the laser fluence increases, the particle concentration as well as the average particle diameter increases. In all cases, the lowest laser fluence corresponds to the lowest particle concentration and the highest fluence corresponds to the highest particle concentration trace. The DHB, CHCA, and SA reflection mode are similar to those reported previously with a metal target [10] and are included for comparison with reflection mode DHAP and NPG.

The particle diameter increases between 15 % and 70 % from the lowest to highest fluence. The average particle diameter and total particle concentration is indicated in Table 1 for the different matrix and laser fluence combinations. The largest average particle diameter was observed for SA, which was more than twice as large as for DHAP and NPG, which had the smallest diameters that were observed. The total particle concentration increases with laser fluence as indicated in Table 1. The largest concentration of particles was produced with NPG matrix, which produced roughly double the particle concentration of the other matrices.

Transmission mode particle number concentration plots for DHB, CHCA, SA, DHAP, and NPG are shown in Figure 2 and the average particle diameter and total particle concentration are indicated in Table 1. The particle diameter and the particle concentration both increase with increasing laser fluence. The total particle concentration is lower in transmission mode than in reflection mode for all of the matrices and all pulse energies by a factor of two to three. For DHB, CHCA, and SA, the particle diameter is slightly smaller in transmission mode: roughly two-thirds as large as the comparable reflection mode configuration. For DHAP, the particle diameter in reflection and transmission mode is similar. NPG had the smallest particle diameter in transmission mode, which was less than half as large as that observed in reflection mode.

Particle mass concentration was recorded for reflection and transmission mode irradiation for each matrix. In these plots, the total mass of particulate material is plotted as a function of particle diameter, which gives an indication of the distribution of ejected mass as a function of particle diameter. The mass concentration for reflection mode is plotted in Figure 3 for matrixes, DHB, CHCA, SA, DHAP, and NPG ablated at fluences of 1400, 1700, 2000, and 2300 J/m^2 (the conditions are identical to those used for the data shown in Figure 1). As reported previously [10], two maxima are observed in the mass concentration plot: smaller particles with diameters in the 100 nm range and larger particles with diameters in the 800 nm range. The small particles represent two to three times as much mass as the large particles. As indicated in Table 1, the mass-weighted average diameter of the small particles ranges from 200 to 300 nm with the exception of DHAP with average diameter less than 100 nm. DHAP is unique in that there appears to be a third maximum in the size distribution near 400 nm at higher laser fluences. The mass-weighted average diameter of the large particles ranges from 700 to 900 nm with the

Table 1. Particle Size and Concentration Values for Matrices DHB, CHCA, SA, DHAP, and NPG

Matrix	Laser fluence (J/m^2)	Average diameter (nm)		Total concentration ($/cm^3$)		Mass-weighted average diameter (reflection)		Mass-weighted total concentration (reflection)		Mass-weighted average diameter (μm)	Mass concentration ($\mu g/m^3$)
		Reflection	Transmission	Reflection	Transmission	<450 nm	>450 nm	<450 nm ($\mu g/m^3$)	>450 nm ($\mu g/m^3$)	Transmission	Transmission
DHB	1400	85	78	48560	16110	245	835	850	420	12	750
	1700	93	68	85440	25950	230	835	1050	580	13	1040
	2000	95	77	100810	39160	245	835	2060	660	14	2600
	2300	98	96	138260	52160	215	770	2720	940	16	3800
CHCA	1400	68	64	24050	9440	170	675	270	50	13	3900
	1700	74	67	51980	18360	185	720	450	110	13	6510
	2000	81	69	82720	40210	200	670	520	320	14	10340
	2300	94	72	97920	66130	265	725	1040	380	16	12200
SA	1400	101	63	38140	27070	200	770	1060	410	12	2660
	1700	116	72	46220	40110	245	900	2100	750	13	4020
	2000	117	81	79420	43630	245	835	2600	880	15	6200
	2300	124	84	96170	51910	265	900	4300	1260	16	7900
DHAP	1400	28	24	65000	17000	65	720	900	630	12	2500
	1700	33	28	10100	29000	70	770	1100	750	13	3100
	2000	41	36	11400	38000	85	835	1500	870	13	4300
	2300	47	42	12500	43000	90	940	1700	1030	14	5600
NPG	1400	32	14	110000	14000	150	970	530	330	16	2600
	1700	38	16	142000	32000	170	1040	950	450	16	2900
	2000	45	19	189000	48000	180	1040	1540	590	16	4700
	2300	47	24	234000	57000	200	1180	2080	900	18	6100

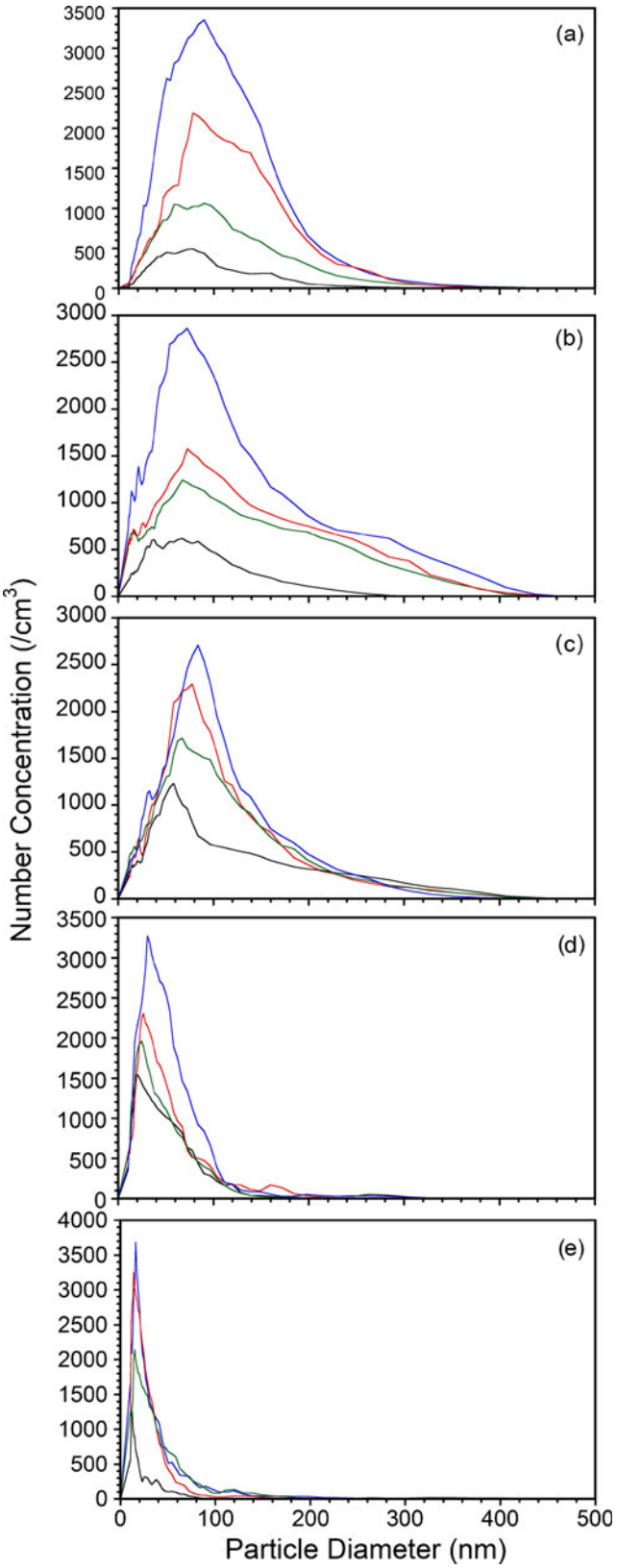

Figure 2. Transmission mode particle size distribution measured in particle count at different laser fluencies increasing from 1400 (black), 1700 (green), 2000 (red,) and 2300 J/m^2 (blue) for matrices: (**a**) DHB, (**b**) CHCA, (**c**) SA, (**d**) DHAP, and (**e**) NPG

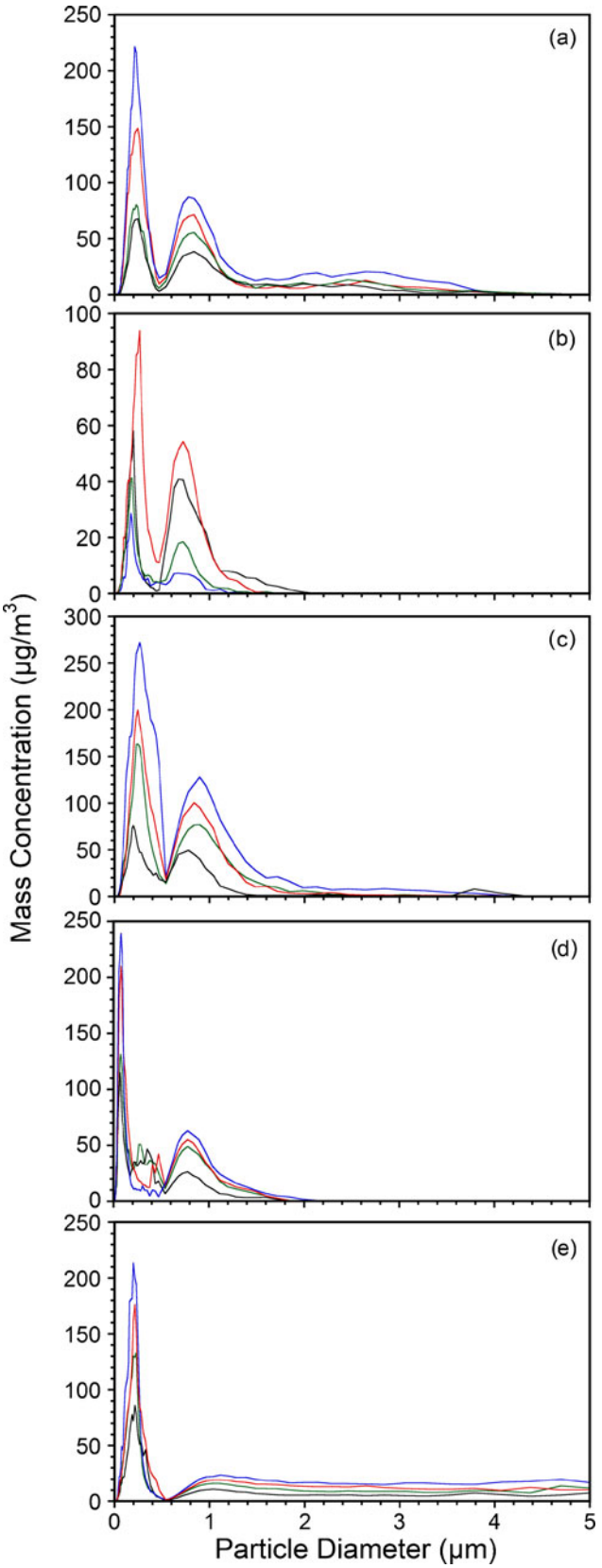

Figure 3. Reflection mode mass weighted particle size distribution for (**a**) DHB, (**b**) CHCA, (**c**) SA, (**d**) DHAP, and (**e**) NPG at laser fluences 1400 (black), 1700 (green), 2000 (red), and 2300 J/m^2 (blue)

exception of NPG, which has a broad distribution of particle sizes that leads to a larger average diameter.

The mass concentration for transmission mode ablation is shown in Figure 4 for matrixes, DHB, CHCA, SA, DHAP, and NPG at fluences of 1400, 1700, 2000, and 2300 J/m^2 that were identical to those above (the conditions were the same as those used to obtain Figure 2). More than 1000 times more mass is ejected as particles greater than 450 nm in diameter compared to the mass ejected as particles with diameters less than 450 nm and the mass weighted particle diameter for the transmission mode ablated particles is larger than those observed in reflection mode ablation. The results are indicated in Table 1; the mass-weighted particle diameters were greater than 10 µm for all matrices and the average diameters are approximately 10 times larger for transmission mode ablation compared to reflection mode ablation. The mass weighted total concentration is larger in transmission mode for all matrices with the exception of DHB, for which the two modes yield results of comparable magnitude.

The main difference between the distribution of particle sizes in reflection and transmission mode is the significantly greater size of the particles produced in transmission mode compared to those produced in reflection mode. The quantity of material ejected is similar, but the size of the particles ejected in transmission mode is approximately ten times larger. The size distribution of particles less than 500 nm in diameter is not significantly different between reflection and transmission ablation.

The reason for the difference in coarse particle size may be related to differences in large particles ejected in back-side compared with front-side ablation. With pulsed ns lasers, there are two distinct mechanisms for material removal: desorption and ablation [16]. At lower fluences, the laser heats the surface relatively slowly, which results in desorption of free molecules. At higher fluences, ablation of clusters and particles occur in part due to explosive boiling (phase explosion) of the superheated material [17–20]. If the sample is heated rapidly to approximately 90 % of the critical temperature, the superheated material can undergo an explosive phase transition that results in volume ejection of the upper layers of the sample.

There is a second distinction that involves the speed at which energy is added to a sample compared with the speed at which it can be removed. Thermal confinement is achieved when heat is added to the system faster than it is removed by thermal diffusion [18]. This occurs under the laser desorption conditions used for MALDI with UV lasers [21]. Stress confinement occurs when the laser adds energy to the system faster than it can be removed through pressure waves and is limited by the speed of sound in the material [18]. Typical vacuum MALDI conditions are not in the stress confinement regime; however, higher laser energies may be sufficient to enter that regime. Explosive boiling can occur under both thermal and stress confinement conditions, but stress confinement tends to produce larger particles.[18, 22]

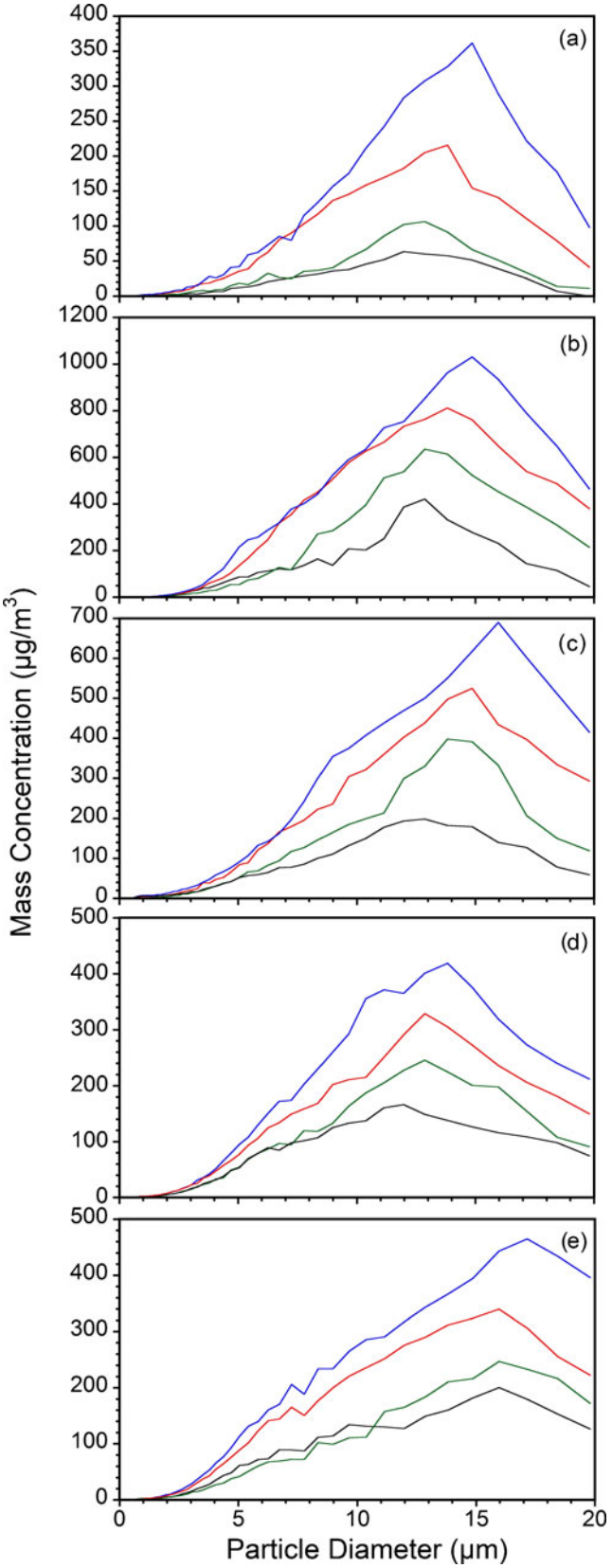

Figure 4. Transmission mode mass weighted particle size distribution for (**a**) DHB, (**b**) CHCA, (**c**) SA, (**d**) DHAP, and (**e**) NPG at laser fluences 1400 (black), 1700 (green), 2000 (red), and 2300 J/m^2 (blue)

Material removal proceeds differently in front and back side irradiation. In reflection mode the surface material absorbs the radiation and material is removed from the top layers. In the stress confinement regime, the shock wave can propagate through the material and reflect back to the surface causing spallation [23]. In transmission mode, the material absorbing the laser radiation is at the bottom of the thin film at the target surface. However, if the lower layers of the sample are heated to the point of vaporization, the gas bubbles from the vaporized sample can form a layer between the substrate and sample [24]. Such a "boiling crisis" (film boiling) phenomenon has been suggested as a means of material ejection in pulsed laser ablation [25]. Large particles may be ejected from the upper layers without significant heating by the laser. The need to remove the upper matrix layer may be related to the higher energy required for transmission mode AP-MALDI compared to reflection mode [26].

The difference between reflection and transmission mode for particles below 450 nm in diameter is not great; however, there is a difference between the matrices that function well for inlet ionization (DHAP and NPG) and those that do not function as well (DHB, CHCA, and SA). The particles produced from ablation of DHAP and NPG have average diameters less than 50 nm both in reflection and transmission mode, whereas the DHB, CHCA, and SA matrices have average diameters ranging from 70 to 125 nm in reflection mode and between 60 and 100 nm in transmission mode. The smallest particles, with average diameters less than 25 nm, are produced from NPG in transmission mode ablation.

It has been suggested that ion formation in laserspray occurs through matrix melting and charge segregation during droplet breakup to form highly charged clusters and nanoparticles [27]. Highly charged ions are then formed through the evaporation of matrix molecules in a manner similar to electrospray. This idea is supported by measurements of laser ablated fluorescent dyes mixed with matrix molecules [28]. It was found that the laser ablated dye molecules were in clusters or particles and no free dye molecules were detected. The fact that the efficient laserspray matrix compounds DHAP and NPG produce smaller particles on ablation is also consistent with this mechanism. The smaller particles will require less time for melting and this is consistent with more efficient ion formation. It should be noted that the particle sizing system used in this work does not detect small molecular clusters: a 10 nm matrix particle contains a few thousand molecules and particles this size and smaller are not detected by the scanning mobility particle sizer.

In addition to small particle charging, it may be possible to create highly charged clusters and nanoparticles by the melting and breakup of large particles on contact with the heated ion source inlet. Particles striking the walls of the capillary inlet will be heated rapidly and smaller particles sheared from the surface could gain charge through a triboelectric mechanism [27] and produce highly charged

ions by matrix evaporation. Without such a surface interaction, is not likely that the material ablated as large particles will result in the production of ions.

Conclusions

Particle size distributions were measured for material ablated from crystalline thin films of matrix compounds used for matrix-assisted ionization. Similar to previous studies of MALDI matrix compounds [10], reflection mode ablation results in a bimodal distribution of particle sizes with small particles averaging between 30 and 120 nm in diameter and an approximately equal mass ejected as large particles approximately 1 μm in diameter. Transmission mode ablation also results in a bimodal distribution, but most of the mass is removed as large particles greater than 10 μm in diameter. The other notable observation is that the matrix compounds that give the best performance for inlet ionization, DHAP and NPG, produce the smallest particles both in reflection and transmission mode. This is particularly notable for NPG in transmission mode where average particle sizes near 20 nm in diameter were recorded.

The observed particle size distributions can be interpreted in the context of proposed mechanisms for inlet ionization [27]. Ion formation is believed to proceed through the evaporation of matrix from highly charged small particles and clusters in a manner similar to electrospray except that the "solvent" is the matrix itself. It has been suggested that non-statistical process during the aerodynamic breakup of melted matrix particles could lead to the highly charged particles and clusters. This hypothesis is consistent with the relatively small size of the particles ablated from the efficient inlet ionization matrices DHAP and NPG. The smaller particles will melt more rapidly and could more quickly fracture, forming small highly charged particles. The large particles may also play a role in ion formation by striking the heated ion source inlet, which could produce highly charged particles through a triboelectric effect or the molten droplets could achieve a high charge through the aerodynamic breakup mechanism.

Additional studies will be necessary to determine whether nanoparticles, coarse particles, or both are responsible for inlet ion formation. One potentially useful avenue is computer simulation. For example, it should be possible to model droplet heating and breakup using finite element computer simulations [29–31] and assess the likelihood of an aerodynamic breakup charging mechanism. Another approach is size selection of particles after their formation but before they enter the ion source inlet, which could reveal the relationship between particle size and ionization efficiency.

References

1. Trimpin, S., Inutan, E.D., Herath, T.N., McEwen, C.N.: Laserspray ionization, a new atmospheric pressure MALDI method for producing highly charged gas-phase ions of peptides and proteins directly from solid solutions. *Mol. Cel. Proteom.* **9**, 362–367 (2010)
2. Trimpin, S., Inutan, E.D., Herath, T.N., McEwen, C.N.: Matrix-assisted laser desorption/ionization mass spectrometry method for selectively producing either singly or multiply charged molecular ions. *Anal. Chem.* **82**, 11–15 (2010)
3. Inutan, E.D., Wang, B., Trimpin, S.: Commercial Intermediate Pressure MALDI Ion mobility spectrometry mass spectrometer capable of producing highly charged laserspray ionization ions. *Anal. Chem.* **83**, 678–684 (2011)
4. Trimpin, S., Ren, Y., Wang, B., Lietz, C.B., Richards, A.L., Marshall, D.D., Inutan, E.D.: Extending the laserspray ionization concept to produce highly charged ions at high vacuum on a time-of-flight mass analyzer. *Anal. Chem.* **83**, 5469–5475 (2011)
5. Overberg, A., Karas, M., Bahr, U., Kaufmann, S., Hillenkamp, F.: Matrix-assisted infrared-laser (2.94 mm) desorption/ionization mass spectrometry of large biomolecules. *Rapid Commun. Mass Spectrom* **4**, 293–296 (1990)
6. Overberg, A., Karas, M., Hillenkamp, F.: Matrix-assisted laser desorption of large biomolecules with a TEA-CO2-Laser. *Rapid Commun. Mass Spectrom.* **5**, 128–131 (1991)
7. Menzel, C., Dreisewerd, K., Berkenkamp, S., Hillenkamp, F.: The role of the laser pulse duration in infrared matrix-assisted laser desorption/ionization mass spectrometry. *J. Am. Soc. Mass Spectrom.* **13**, 975–984 (2002)
8. McEwen, C.N., Trimpin, S.: An alternative ionization paradigm for atmospheric pressure mass spectrometry: Flying elephants from Trojan horses. *Int. J. Mass Spectrom.* **300**, 167–172 (2011)
9. Zilch, L.W., Maze, J.T., Smith, J.W., Ewing, G.E., Jarrold, M.F.: Charge separation in the aerodynamic breakup of micrometer-sized water droplets. *J. Phys. Chem. A* **112**, 13352–13363 (2008)
10. Musapelo, T., Murray, K.K.: Particle formation in ambient MALDI Plumes. *Anal. Chem* **83**, 6601–6608 (2011)
11. Alves, S., Kalberer, M., Zenobi, R.: Direct detection of particles formed by laser ablation of matrices during matrix-assisted laser desorption/ionization. *Rapid. Commun. Mass. Spectrom.* **17**, 2034–2038 (2003)
12. Jackson, S.N., Mishra, S., Murray, K.K.: Characterization of coarse particles formed by laser ablation of MALDI matrixes. *J. Phys. Chem. B* **107**, 13106–13110 (2003)
13. Kim, J.-K., Jackson, S.N., Murray, K.K.: Matrix-assisted laser desorption/ionization mass spectrometry of collected bioaerosol particles. *Rapid Commun. Mass Spectrom.* **19**, 1725–1729 (2005)
14. Fan, X., Little, M.W., Murray, K.K.: Infrared laser wavelength dependence of particles ablated from glycerol. *Appl. Surf. Sci* **255**, 1699–1704 (2008)
15. Li, J., Inutan, E.D., Wang, B., Lietz, C.B., Green, D.R., Manly, C.D., Richards, A.L., Marshall, D.D., Lingenfelter, S., Ren, Y., Trimpin, S.: Matrix assisted ionization: New aromatic and nonaromatic matrix compounds producing multiply charged lipid, peptide, and protein ions in the positive and negative mode observed directly from surfaces. *J. Am. Soc. Mass Spectrom.* **23**, 1625–1643 (2012)
16. Zhigilei, L.V., Yingling, Y.G., Itina, T.E., Schoolcraft, T.A., Garrison, B.J.: Molecular dynamics simulations of matrix-assisted laser desorption-connections to experiment. *Int. J. Mass. Spectrom.* **226**, 85–106 (2003)
17. Miotello, A., Kelly, R.: Laser-induced phase explosion: New physical problems when a condensed phase approaches the thermodynamic critical temperature. *Appl. Phys. A* **69**, S67–S73 (1999)
18. Zhigilei, L.V., Garrison, B.J.: Microscopic mechanisms of laser ablation of organic solids in the thermal and stress confinement irradiation regimes. *J. Appl. Phys.* **88**, 1281–1298 (2000)
19. Apitz, I., Vogel, A.: Material ejection in nanosecond Er:YAG laser ablation of water, liver, and skin. *Appl. Phys. A* **81**, 329–338 (2005)
20. Vogel, A., Venugopalan, V.: Mechanisms of pulsed laser ablation of biological tissues. *Chem. Rev.* **103**, 577–644 (2003)
21. Knochenmuss, R., Zhigilei, L.V.: Molecular dynamics model of ultraviolet matrix-assisted laser desorption/ionization including ionization processes. *J. Phys. Chem. B* **109**, 22947–22957 (2005)
22. Leisner, A., Rohlfing, A., Rohling, U., Dreisewerd, K., Hillenkamp, F.: Time-resolved imaging of the plume dynamics in infrared matrix-assisted laser desorption/ionization with a glycerol matrix. *J. Phys. Chem. B* **109**, 11661–11666 (2005)
23. Zhigilei, L.V., Ivanov, D.S., Leveugle, E., Sadigh, B., Bringa, E.M.: Computer simulations of laser ablation from simple metals to complex metallic alloys. *Proceedings of SPIE* **5448**, 505–519 (2004)

24. Nikolayev, V.S., Beysens, D.A.: Boiling crisis and non-equilibrium drying transition. *Europhys. Lett.* **47**, 345–351 (1999)
25. Bulgakova, N.M., Bulgakov, A.V.: Pulsed laser ablation of solids: Transition from normal vaporization to phase explosion. *Appl. Phys. A* **73**, 199–208 (2001)
26. Galicia, M., Vertes, A., Callahan, J.: Atmospheric pressure matrix-assisted laser desorption/ionization in transmission geometry. *Anal. Chem.* **74**, 1891–1895 (2002)
27. Trimpin, S., Wang, B., Inutan, E.D., Li, J., Lietz, C.B., Harron, A., Pagnotti, V.S., Sardelis, D., McEwen, C.N.: A mechanism for ionization of nonvolatile compounds in mass spectrometry: Considerations from MALDI and inlet ionization. *J. Am. Soc. Mass Spectrom.* **23**, 1644–1660 (2012)
28. Frankevich, V., Nieckarz, R.J., Sagulenko, P.N., Barylyuk, K., Zenobi, R., Levitsky, L.I., Agapov, A.Y., Perlova, T.Y., Gorshkov, M.V., Tarasova, I.A.: Probing the mechanisms of ambient ionization by laser-induced fluorescence spectroscopy. *Rapid Commun. Mass Spectrom.* **26**, 1567–1572 (2012)
29. Costa, A.B.; Cooks, R.G.: Simulation of atmospheric transport and droplet-thin film collisions in desorption electrospray ionization. *Chem. Commun*. 3915–3917. doi:10.1039/b710511h (2007)
30. Costa, A.B., Cooks, R.G.: Simulated splashes: Elucidating the mechanism of desorption electrospray ionization mass spectrometry. *Chem. Phys. Lett.* **464**, 1–8 (2008)
31. Huang, F., Murray, K.K.: Finite element simulation of infrared laser ablation for mass spectrometry. *Rapid Commun. Mass Spectrom.* **26**, 2145–2150 (2012)